

# Deep Scatter Splines: Learning-Based Medical X-ray Scatter Estimation Using B-splines

Philipp Roser, Annette Birkhold, Alexander Preuhs, Christopher Syben, Norbert Strobel, Markus Korwarschik, Rebecca Fahrig, Andreas Maier

**Abstract**—The idea of replacing hardware by software to compensate for scattered radiation in flat-panel X-ray imaging is well established in the literature. Recently, deep-learning-based image translation approaches, most notably the U-Net, have emerged for scatter estimation. These yield considerable improvements over model-based methods. Such networks, however, involve potential drawbacks that need to be considered. First, they are trained in a data-driven fashion without making use of prior knowledge and X-ray physics. Second, due to their high parameter complexity, the validity of deep neural networks is difficult to assess. To circumvent these issues, we introduce here a surrogate function to model X-ray scatter distributions that can be expressed by few parameters. We could show empirically that cubic B-splines are well-suited to model X-ray scatter in the diagnostic energy regime. Based on these findings, we propose a lean convolutional encoder architecture that extracts local scatter characteristics from X-ray projection images. These characteristics are embedded into a global context using a constrained weighting matrix yielding spline coefficients that model the scatter distribution. In a first simulation study with 17 thorax data sets, we could show that our method and the U-Net-based state of the art reach about the same accuracy. However, we could achieve these comparable outcomes with orders of magnitude fewer parameters while ensuring that not high-frequency information gets manipulated.

**Index Terms**—Splines, Neural Network, X-ray Scatter.

## I. INTRODUCTION

**F**LAT-PANEL detector cone-beam computed tomography (CBCT) is a powerful technique to enrich fluoroscopically-guided interventions (FGI) with 3-D information of a patient’s anatomy. In contrast to conventional spiral computed tomography (CT), flat-panel X-ray acquisitions suffer, due to the larger X-ray field, from severe photon scattering effects. Without scatter compensation, reconstructed 3D images are likely to be impaired by streaking or cupping artifacts [1], [2]. In principal, two compensation strategies are possible: hardware-based and software-based approaches.

Hardware-based solutions describe direct manipulations of the X-ray field to either suppress incident scatter or modulate the primary beam. Typically, today’s systems are equipped with anti-scatter grids mounted in front of the detector. They

physically block a large portion of incoming scattered photons [3]. By increasing the object-detector-distance, scatter can be reduced as well. More sophisticated, experimental approaches include primary modulation [4] and slit scanning [5]. In general, and especially for interventional imaging, hardware-based solutions may complicate flexible adjustment of imaging settings or introduce artifacts of their own [6]. Therefore, and since hardware-based approaches are often accompanied by supporting algorithms in most cases anyways, purely software-based scatter correction methods are very desirable.

As in many applications, Monte Carlo (MC) simulation is considered the gold standard for scatter estimation [7], [8]. Its high computational complexity, however, still renders the actual application of MC simulation for scatter estimation in the interventional environment impracticable. As a solution, the Boltzmann transport equation can be solved directly using finite differences and discretization [9]. Yet, an acceptable run-time is only achievable by employing dedicated graphics processing units (GPU). This is why simpler, model-based approaches are still most widely used in clinical systems. They aim at estimating scatter from the X-ray projections directly, and are either based on simplified physical or analytical descriptions of X-ray scattering [10], [11] or expressed through convolutional kernels [12]. Unfortunately, model-based approaches are likely to fail if acquired images do not meet the underlying assumptions.

With the advent of convolutional neural networks (CNN) and most notably the U-Net [13] in the context of image-to-image translation, promising advances in the field of X-ray scatter correction were reported [14], [15]. The Deep Scatter Estimation (DSE) framework [14] is, for example, able to estimate X-ray scatter solely based on X-ray projections. In fact, it is on par with MC methods under optimal simulation conditions. However, the application of deep CNNs for image-to-image translation, especially in diagnostic imaging or FGIs, raises questions that are difficult to answer. Besides the overall difficulty in comprehending the operating principle of deep networks, the large number of trainable weights makes the U-Net highly dependent on the associated training data and therefore prone to adversarial effects and over-fitting. In addition, omitting prior knowledge can lead to higher maximum error bounds [16]. Finally, to maintain a fast run-time, U-Net-based scatter estimation is likely to require a dedicated, high-end GPU potentially adding considerable extra cost to the system.

We believe that by including additional constraints on the scatter characteristics within a CNN-based approach, improvements can be achieved. Since in the medical X-ray energy

P. Roser, A. Preuhs, C. Syben, and A. Maier are with the Pattern Recognition Lab, Department of Computer Science, Friedrich-Alexander Universität Erlangen-Nürnberg, Erlangen, Germany. P. Roser is funded by the Erlangen Graduate School in Advanced Optical Technologies (SAOT), Friedrich-Alexander Universität Erlangen-Nürnberg, Erlangen, Germany. A. Maier is principal investigator at the SAOT. A. Birkhold, M. Kowarschik, and R. Fahrig are employees of Siemens Healthcare GmbH, 91301 Forchheim, Germany. N. Strobel is with the Institute of Medical Engineering Schweinfurt, University of Applied Sciences WürzburgSchweinfurt, 97421 Schweinfurt, Germany.

regime the majority of scattered radiation is low-frequency, there needs to exist a low-dimensional scatter representation. Here, we show that this low-frequency scatter distribution can be approximated by sparse bivariate splines [17] with an accuracy of up to 98%. To this end, we train a CNN-based encoder to directly infer this representation from X-ray projections. Thanks to the spline approximation, the number of parameters to train could be reduced by orders of magnitude, while maintaining the accuracy of the established U-Net. By using a low-dimensional spline as surrogate, we also ensure low-frequency characteristics of the resulting scatter distribution. As a consequence, the proposed method cannot alter any high-frequency information because it is simply removing a smoothly varying background.

## II. MATERIAL AND METHODS

### A. X-ray Scatter Model

In general, three photon interaction mechanisms are relevant for scatter in X-ray projections: (1) Rayleigh scattering, (2) Compton scattering, and (3) arbitrary, subsequent combinations of both, related as multiple scattering. Although each of them is subject to typical photon Poisson noise, the total scatter distribution in X-ray projections has low-frequency characteristics. In the following, we consider the flat-field normalized X-ray projection  $\mathbf{I} \in \mathbb{R}^{w \times h}$  with width  $w$  and height  $h$  in pixels. The X-ray projection consists of the primary signal  $\mathbf{I}_p \in \mathbb{R}^{w \times h}$  described using the Beer-Lambert law and scatter  $\mathbf{I}_s \in \mathbb{R}^{w \times h}$ . The scatter signal includes all scattering mechanisms. Thus  $\mathbf{I}$  at pixel  $\mathbf{u} = (u_w, u_h)$  is given by

$$\mathbf{I}(\mathbf{u}) = \underbrace{\int_E I_0(E) e^{-\int_x \mu(x,E) dx} dE}_{\mathbf{I}_p(\mathbf{u})} + \mathbf{I}_s(\mathbf{u}), \quad (1)$$

with the photon energy  $E$ , X-ray spectrum  $I_0(E)$ , and the linear attenuation coefficient  $\mu(x, E)$ .

We approximate  $\mathbf{I}_s$  at pixel  $\mathbf{u}$  using a bivariate spline of degree  $k$  and order  $n = k + 1$ . The spline is defined by a  $w_c \times h_c$  grid of coefficients  $\mathbf{C} \in \mathbb{R}^{w_c \times h_c}$  on a fixed knot grid  $\mathbf{T} \in \mathbb{R}^{(w_c-k+1) \times (h_c-k+1)}$ . This gives us the surrogate  $\tilde{\mathbf{I}}_{s,n}(\mathbf{u})$  at pixel  $\mathbf{u} = (u_0, u_1)$

$$\tilde{\mathbf{I}}_{s,n}(\mathbf{u}) = \sum_{i=i_0}^{n+i_0} \sum_{j=j_0}^{n+j_0} \mathbf{C}_{i,j} B_{i,n,\mathbf{T}}(u_0) B_{j,n,\mathbf{T}}(u_1), \quad (2)$$

with the basis splines  $B$ . Note that the starting indices  $i_0$  and  $j_0$  depend on both the evaluated pixel  $\mathbf{u}$  and the knot grid  $\mathbf{T}$ . Since  $\mathbf{T}$  is fixed for any X-ray projection, we fit the associated splines in a least-square sense, following Dierckx [18]. The error residual  $\varepsilon_r = \|\mathbf{I}_s - \tilde{\mathbf{I}}_{s,n}\|_2$  approaches 0 with increasing number of spline coefficients.

### B. Proposed Method

Based on our scatter model, we propose to infer scatter spline coefficients directly from the X-ray projection domain. The outline of the presented method is depicted in Fig. 1. From ground truth MC scatter simulations, we find a sparse scatter representation by fitting bivariate splines with respect

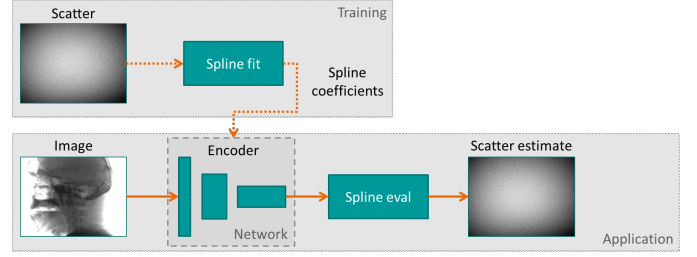


Fig. 1. Overview of the proposed method. Ground truth scatter distributions are approximated using bivariate B-splines. Then a convolutional encoder is trained to directly infer spline coefficients from the projection image. Afterwards, these spline coefficients are used to calculate the actual scatter distribution of the underlying input image.

to an arbitrary but fixed knot grid  $\mathbf{T}$ . The resulting spline coefficients  $\mathbf{C}$  are then used to train a deep encoder to extract such a sparse scatter representations from an X-ray projection. By evaluating the inferred spline coefficients using the previously defined grid, we are able to obtain the low-frequency portion of scatter distributions for any desired pixel spacing.

The encoder employed consists of blocks of two convolutional layers, each followed by a rectified linear unit (ReLU). The number of blocks is arbitrary and manually adjustable to the input and output dimensions. Between two convolutional blocks, the dimensions of the feature maps are halved by averaging a neighborhood of  $2 \times 2$  pixels for each feature map. The number of intermediate feature maps is constant for all levels. Before each convolution, replication padding is applied to preserve spatial dimensions. The last block is followed by a weighted sum over all channels to reduce the number of intermediate channels to one. Eventually, the latent variable of width  $w_l$  and height  $h_l$  is vectorized. This convolutional path  $\mathcal{S}_\theta : \mathbb{R}^{w \times h} \mapsto \mathbb{R}^{w_l \cdot h_l \times 1}$  extracts latent variables that locally characterize X-ray scattering. However, scattered radiation globally affects image formation. To account for this, we model each spline coefficient  $C_{i,j}$  as the weighted, normalized sum of all intermediate latent variables. This global relationship can be expressed by multiplying the latent variable with matrix  $\mathbf{W} \in \mathbb{R}^{w_c \cdot h_c \times w_l \cdot h_l}$ , which is only feasible due to the low dimensionality of the latent space and not directly transferable to the DSE.

To be comparable to the DSE, the network parameters  $\theta$  and  $\mathbf{W}$  are optimized by minimizing the mean absolute percentage error (MAPE) with respect to the ground truth

$$\theta, \mathbf{W} = \arg \min_{\theta, \mathbf{W}} \sum_i \sum_j \frac{\|[\mathbf{W} \mathcal{S}_\theta(\mathbf{I})]_{i,j} - C_{i,j}\|_1}{C_{i,j}}, \quad (3)$$

where  $[\cdot]_{i,j}$  is the access operation for a vectorized matrix. Since  $\mathbf{W}$  models a weighted sum, we impose two constraints: (1) each element of  $\mathbf{W}$  must be positive  $W_{i,j} > 0, \forall i, j$  and (2) each row sums up to unity  $\sum_j W_{i,j} = 1, \forall i$ .

### C. Ground Truth Data Simulation

Acquiring matching pairs of training data using conventional X-ray imaging is tedious and time-consuming. As an

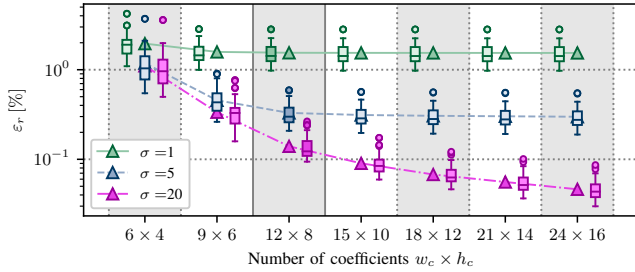


Fig. 2. Absolute average spline approximation error  $\varepsilon_r$  (triangles) and associated box plots for different numbers of coefficients for strong ( $\sigma = 20$ ), medium ( $\sigma = 5$ ), and no ( $\sigma = 1$ ) Gaussian smoothing.

alternative, we used the X-ray transport code MC-GPU [19] to generate synthetic training data. As inputs for our simulation, openly accessible CT scans from The Cancer Imaging Archive (TCIA) [20] were used. In total, we extracted 17 thorax phantoms from the CT Lymph Nodes torso [21] data sets. To prepare the phantoms for MC simulation, we employed a basic pre-processing pipeline [22] to remove non-patient objects, and assign tissues and densities to each voxel. Based on the simulated scatter distributions, we fit bivariate cubic B-splines.

For each X-ray projection, we simulated  $5 \times 10^{10}$  primary photons sampled from a 100 keV tungsten spectrum. In total, we considered three slightly different iso-center positions  $\mathbf{o} \in \mathbb{R}^3$ , seven different projection angles  $\alpha \in \{0, 15, 30, \dots, 90\}$  in  $^\circ$ , and fixed source-to-detector (1300 mm) and source-to-iso-center (800 mm) distances, respectively. The virtual detector is  $399 \text{ mm} \times 299 \text{ mm}$  large and consists of  $1248 \times 928$  pixels. To reduce simulation noise, we filter the scatter signals using a Gaussian kernel  $G_\sigma$ .

### III. RESULTS

#### A. Spline Approximation Capability

Initially, we investigated the quality of splines for medical X-ray scatter approximation. To this end, we fit cubic splines ( $k = 3$ ) with a different number of coefficients  $\mathbf{C} \in \mathbb{R}^{w_c \times h_c}$  to the scatter signal and juxtaposed the associated residuals  $\varepsilon_r$ . Figure 2 summarizes the results for  $w_c \times h_c \in \{48 \times 32, 24 \times 16, 12 \times 8, 6 \times 4, 3 \times 2\}$  for all considered simulated X-ray scatter signals. Evidently, only marginal improvements can be observed with increasing number of coefficients. The best trade-off between sparsity and a low approximation error was obtained with  $12 \times 8$  coefficients. Hence, we considered  $\mathbf{C} \in \mathbb{R}^{12 \times 8}$  for further analysis.

#### B. Experimental Setup

In accordance to the DSE [14], our encoder network is trained with down-sampled X-ray projections comprising  $384 \times 256$  pixels and targets  $12 \times 8$  spline coefficients. We excluded one patient for validation during training ( $1 \times 21$  X-ray projections) and one patient for testing afterwards ( $2 \times 21$  X-ray projections). Hence, the encoder was trained using 273 X-ray projections from 13 patients and a batch size of 16. For data augmentation, we used random horizontal flips and

TABLE I  
NUMBER OF PARAMETERS TO TRAIN AND QUANTITATIVE TEST RESULTS FOR ALL INVESTIGATED NETWORK ARCHITECTURES FOR DIFFERENT DEPTHS  $d$  AND NUMBER OF FEATURE MAPS  $c$ . FOR BETTER ASSESSMENT, THE MEDIAN ABSOLUTE PERCENTAGE ERROR (MEDAPE) IS ALSO GIVEN.

Architecture	$d$	$c$	Parameters	MAPE [%]	MedAPE [%]
U-Net	6	8	12.6M	4.66(409)	3.59
		16	50.3M	5.06(389)	4.24
	5	8	3.1M	5.04(425)	3.97
		16	12.6M	5.41(413)	4.60
Ours	7	8	10.1k	4.84(401)	3.80
		16	32.7k	4.53(382)	3.51
	6	8	15.8k	4.66(422)	3.55
		16	35.0k	4.67(429)	3.65

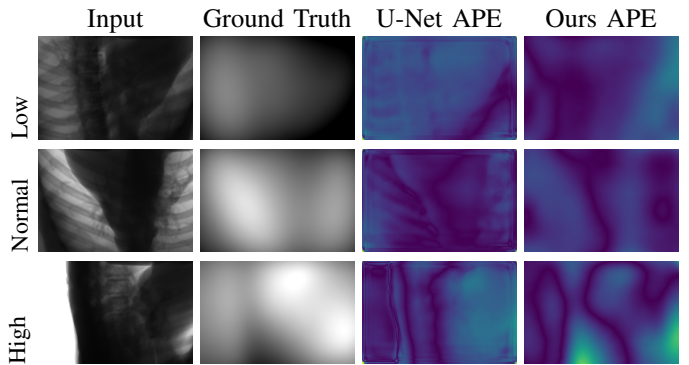


Fig. 3. Qualitative comparison between both approaches for three different views of different intensity ranges (low, normal, high). Input and ground truth are windowed to give a good visual representation. Absolute percentage errors (APE) are in the range of 0% to 25% (dark blue to yellow).

random Poisson noise as these techniques preserve physical plausibility. The network was trained using adaptive moments optimizer with default parameters [23] subject to minimize the MAPE to the target MC scatter simulations. The results were compared to the U-Net with respect to the ground truth MC scatter simulations. We trained the baseline U-Net and our network architecture with different depths  $d$  and number of initial feature maps  $c$  (see Tab. I).

#### C. Comparison of the Network Architectures

Table I shows the pixel-wise MAPE with respective standard deviations and the median absolute percentage error (MedAPE) of the investigated network architectures on the two test patients. Evidently, both network architectures perform similarly for all parameter combinations and median error rates range from 3.55% to 4.60%. However, slight trends can be observed. The U-Net configurations with fewer parameters (8 initial feature maps) yield 0.64% lower median error rates on average compared to their high-parameters counterparts. Such a trend is not seen for our network architecture. Furthermore, it reaches overall lower error rates on average compared to the U-Net. Most strikingly, our method is capable to maintain the U-Net's accuracy while reducing the number of parameters to train by two to three orders of magnitude.

To assess the network architectures from a qualitative point of view, Fig. 3 depicts three example projections, their associ-

ated scatter signals, and the absolute percentage errors (APE) of the predictions by the U-Net ( $d = 6, c = 8$ ) and our encoder ( $d = 7, c = 16$ ) with respect to the ground truth. Overall, the scatter distributions are smooth and almost no salient features are observable, in particular in the proposed approach.

#### IV. DISCUSSION AND CONCLUSION

We developed a novel method to estimate X-ray scatter from projection images in a data-driven fashion. Leveraging the ability of B-splines to approximate low-frequency signals, we were able to tremendously reduce the number of training parameters to arrive at results comparable to the current state of the art. We presented a proof of concept based on a simulation study involving 17 thorax data sets at one fixed peak tube voltage relevant for medical X-ray diagnostics.

Although these preliminary results appear promising, several limitations of our study need to be discussed. First, as advanced pre-processing has shown potential to improve learning-based scatter estimation by approximately 4% [14] as well, future studies need to incorporate different pre-processing techniques in the evaluation. Second, at this point in time we cannot yet make a statement on how 3D reconstruction benefits, as associated experimental results are not yet available. Third, in contrast to the DSE [14], we only considered one anatomic region and one tube peak voltage. Therefore, no assumption on our method's generalizability to other anatomic regions and X-ray energy regimes can be made. It cannot be ruled out that our lean encoder architecture does not have the same capacity as the U-Net.

Besides these potential limitations, our method comes with interesting characteristics that are very desirable in the interventional environment. First, the parameter reduction leads to a lower computational complexity. This allows for (a) accelerated reconstruction, (b) seamless transition between 3D and 2D imaging, and (c) it can be implemented on a wide variety of processing hardware. In addition, it is questionable whether a single network is needed that can adapt to highly varying tube voltages and anatomic regions. Multiple dedicated networks could be used instead. Second, by using a sparse spline as surrogate signal, our method ensures that only low frequencies get altered in the X-ray projection image. Hence, it is very unlikely that potentially diagnostically relevant anatomic features get removed.

In sum, the use of splines as X-ray scatter surrogate signal has the potential to improve learning-based X-ray scatter estimation algorithms, as it requires significantly fewer parameters and much reduced computational complexity.

**Disclaimer:** The concepts and information presented are based on research and are not commercially available.

#### REFERENCES

[1] E.-P. Rührschopf and K. Klingenbeck, "A general framework and review of scatter correction methods in x-ray cone-beam computerized tomography. part 1: Scatter compensation approaches," *Med Phys*, vol. 38, no. 7, pp. 4296–4311, 2011.  
 [2] —, "A general framework and review of scatter correction methods in cone-beam ct. part 2: Scatter estimation approaches," *Med Phys*, vol. 38, no. 9, pp. 5186–5199, 2011.

[3] H.-P. Chan, Y. Higashida, and K. Doi, "Performance of antiscatter grids in diagnostic radiology: Experimental measurements and monte carlo simulation studies," *Med Phys*, vol. 12, no. 4, pp. 449–454, 1985.  
 [4] B. Bier, M. Berger, A. Maier, M. Kachelrieß, L. Ritschl, K. Müller, J.-H. Choi, and R. Fahrig, "Scatter correction using a primary modulator on a clinical angiography c-arm ct system," *Med Phys*, vol. 44, no. 9, pp. 125–137, 2017.  
 [5] R. Bhagatani and T. G. Schmidt, "Simulated scatter performance of an inverse-geometry dedicated breast ct system," *Med Phys*, vol. 36, no. 3, pp. 788–796, 2009.  
 [6] D. M. Gauntt and G. T. Barnes, "Grid line artifact formation: A comprehensive theory," *Med Phys*, vol. 33, no. 6, pp. 1668–1677, 2006.  
 [7] W. Zbijewski and F. J. Beekman, "Fast scatter estimation for cone-beam x-ray ct by combined monte carlo tracking and richardson-lucy fitting," in *IEEE Nucl Sci Symp Conf Rec*, vol. 5, 2004, pp. 2774–2777.  
 [8] G. Poludniowski, P. M. Evans, V. N. Hansen, and S. Webb, "An efficient monte carlo-based algorithm for scatter correction in keV cone-beam CT," *Phys Med Biol*, vol. 54, no. 12, pp. 3847–3864, 2009.  
 [9] A. Wang, A. Maslowski, P. Messmer, M. Lehmann, A. Strzelecki, E. Yu, P. Paysan, M. Brehm, P. Munro, J. Star-Lack, and D. Seghers, "Acurosc cts: A fast, linear boltzmann transport equation solver for computed tomography scatter part ii: System modeling, scatter correction, and optimization," *Med Phys*, vol. 45, no. 5, pp. 1914–1925, 2018.  
 [10] W. Yao and K. W. Leszczynski, "An analytical approach to estimating the first order scatter in heterogeneous medium. ii. a practical application," *Med Phys*, vol. 36, no. 7, pp. 3157–3167, 2009.  
 [11] M. Meyer, W. A. Kalender, and Y. Kyriakou, "A fast and pragmatic approach for scatter correction in flat-detector CT using elliptic modeling and iterative optimization," *Phys Med Biol*, vol. 55, no. 1, pp. 99–120, 2009.  
 [12] B. Ohnesorge, T. Flohr, and K. Klingenbeck-Regn, "Efficient object scatter correction algorithm for third and fourth generation ct scanners," *Eur Radiol*, vol. 9, no. 3, pp. 563–569, Mar 1999.  
 [13] O. Ronneberger, P. Fischer, and T. Brox, "U-Net: Convolutional networks for biomedical image segmentation," in *Med Image Comput Comput Assist Interv*, ser. Lecture notes in computer science, vol. 9351. Springer, 2015, pp. 234–241.  
 [14] J. Maier, E. Eulig, T. Vöth, M. Knaup, J. Kuntz, S. Sawall, and M. Kachelrieß, "Real-time scatter estimation for medical CT using the deep scatter estimation: Method and robustness analysis with respect to different anatomies, dose levels, tube voltages, and data truncation," *Med Phys*, vol. 46, no. 1, pp. 238–249, 2019.  
 [15] P. Roser, X. Zhong, A. Birkhold, N. Strobel, M. Kowarschik, R. Fahrig, and A. Maier, "Physics-driven learning of x-ray skin dose distribution in interventional procedures," *Med Phys*, vol. 46, no. 10, pp. 4654–4665, 2019.  
 [16] A. Maier, C. Syben, B. Stimpel, T. Wrfl, M. Hoffmann, F. Schebesch, W. Fu, L. Mill, L. Kling, and S. Christiansen, "Learning with known operators reduces maximum error bounds," *Nat Mach Intell*, vol. 1, pp. 373–380, 2019.  
 [17] I. J. Schoenberg, "Contributions to the problem of approximation of equidistant data by analytic functions," *Quart Appl Math*, vol. 4, pp. 45–99, 1946.  
 [18] P. Dierckx, *Curve and Surface Fitting with Splines*. New York, NY, USA: Oxford University Press, Inc., 1993.  
 [19] A. Badal and A. Badano, "Accelerating Monte Carlo simulations of photon transport in a voxelized geometry using a massively parallel graphics processing unit," *Med Phys*, vol. 36, no. 11, pp. 4878–4880, 2009.  
 [20] K. Clark, B. Vendt, K. Smith, J. Freymann, J. Kirby, P. Koppel, S. Moore, S. Phillips, D. Maffitt, M. Pringle, L. Tarbox, and F. Prior, "The Cancer Imaging Archive (TCIA): Maintaining and operating a public information repository," *J Digit Imaging*, vol. 26, pp. 1045–1057, 07 2013.  
 [21] H. Roth, L. Le, S. Ari, K. Cherry, J. Hoffman, S. Wang, and R. Summers, "A new 2.5 d representation for lymph node detection in ct. the cancer imaging archive," 2018. [Online]. Available: <http://doi.org/10.7937/K9/TCIA.2015.AQIIDCNM>  
 [22] P. Roser, A. Birkhold, A. Preuhs, B. Stimpel, C. Syben, N. Strobel, M. Kowarschik, R. Fahrig, and A. Maier, "Fully-automatic ct data preparation for interventional x-ray skin dose estimation," in *Bildverarbeitung für die Medizin*, 03 2020, pp. 125–130.  
 [23] D. Kingma and J. Ba, "Adam: A method for stochastic optimization," in *Proceedings of the International Conference on Learning Representations (ICLR)*, 12 2014.